Han et al. *NPG Asia Materials* (2024)16:9
https://doi.org/10.1038/s41427-024-00529-9

NPG Asia Materials

ARTICLE Open Access

Manipulation of the magnetic monopole injection for topological transition

Hee-Sung Han[1,2], Sergio A. Montoya[3], Eric E. Fullerton[3], Weilun Chao[1], Soong-Geun Je[4], Ki-Suk Lee[5,6] and Mi-Young Im[1]

Abstract

Manipulating the topological properties of spin textures in magnetic materials is of great interest due to the rich physics and promising technological applications of these materials in advanced electronic devices. A spin texture with desired topological properties can be created by magnetic monopole injection, resulting in topological transitions involving changes in the topological charge. Therefore, controlling magnetic monopole injection has paramount importance for obtaining the desired spin textures but has not yet been reported. Here, we report the use of reliably manipulated magnetic monopole injection in the topological transition from stripe domains to skyrmions in an Fe/Gd multilayer. An easily tunable in-plane magnetic field applied to an Fe/Gd multilayer plays a key role in the magnetic monopole injection by modulating the local exchange energy. Our findings facilitate the efficient management of topological transitions by providing an important method for controlling magnetic monopole injection.

Introduction

Spin textures such as skyrmions are classified by their nonzero topological charge $Q = 1/4\pi\int\int \mathbf{m}(\frac{\partial \mathbf{m}}{\partial x} \times \frac{\partial \mathbf{m}}{\partial y})d^2\mathbf{r}$[1,2], where $\mathbf{m}$ is the magnetization unit vector. According to a topological viewpoint, a continuous transformation between topologically distinct spin textures with different Q values is not allowed; thus, spin textures with $Q \neq 0$ have high stability in magnetic medium despite their small size[3–6]. Due to the topology-associated intriguing physical behaviors and unique features of spin textures with $Q \neq 0$, such as skyrmion Hall effects[7,8] and topological protection[3–6], the topological transition from topologically trivial spin textures ($Q = 0$) to non-trivial textures ($Q \neq 0$) has not only attracted significant scientific interest but also been considered important in the development of advanced spin-based electronic devices such as memory, logic, and bioinspired computing devices[9–12].

The topological transition can occur by the discontinuous deformation of the magnetization configuration[1,13,14]. The magnetic monopole (MP)-mediated topological transition is a representative example. The MP is a topological magnetic singularity with $|Q| = 1$ at which the local magnetization vanishes; this singularity is called the Bloch point[15–21]. MP has been the key to elucidating various topological transitions in nanomagnetism[22–24]. For instance, the MP is responsible for the topological transition from the vortex-antivortex pair characterized by $|Q| = 1$ to the topologically trivial state of $|Q| = 0$[25–28]. The vortex–antivortex pair is annihilated through the injection of MP from the surface of a magnetic medium; thus, $|Q|$ of the total system is changed from $|Q| = 1$ to $|Q| = 0$. MP injection also plays an essential role in the merging of two skyrmions ($|Q| \neq 0$) into the stripe domain ($|Q| = 0$) or breaking the stripe domain ($|Q| = 0$) into multiple skyrmions ($|Q| \neq 0$)[29,30].

Despite the central importance of the MP in topological transitions, an efficient means of injecting the MP in a

Correspondence: Hee-Sung Han (hs.han@ut.ac.kr) or Soong-Geun Je (sg.je@chonnam.ac.kr) or Ki-Suk Lee (kisuk@unist.ac.kr) or Mi-Young Im (mim@lbl.gov)
[1]Center for X-ray Optics, Lawrence Berkeley National Laboratory, Berkeley, CA 94720, USA
[2]Department of Materials Science and Engineering, Korea National University of Transportation, Chungju 27469, Republic of Korea
Full list of author information is available at the end of the article

controlled manner has not been addressed yet. In addition, the mechanism for topological transition associated with MP injection and relevant physics are not comprehensively understood. Here, we demonstrate a simple yet robust method for the controlled MP injection that efficiently triggers the topological transition from stripe domains with $Q = 0$ to skyrmions with $|Q| = 1$ in a $[Fe(0.34\,nm)/Gd(0.4\,nm)]_{120}$ ferrimagnetic multilayer film (hereafter referred to as the Fe/Gd multilayer). We reveal that a slight in-plane (IP) magnetic field results in an intense concentration of the local exchange energy, causing an easier MP injection. The Fe/Gd multilayer was chosen because this material has different types of spin textures, topologically trivial stripe domains and magnetic bubbles (hereafter, bubbles), as well as topologically non-trivial skyrmions stabilized by dipole–dipole interactions without Dzyaloshinskii-Moriya interactions (DMIs)[6,31–34].

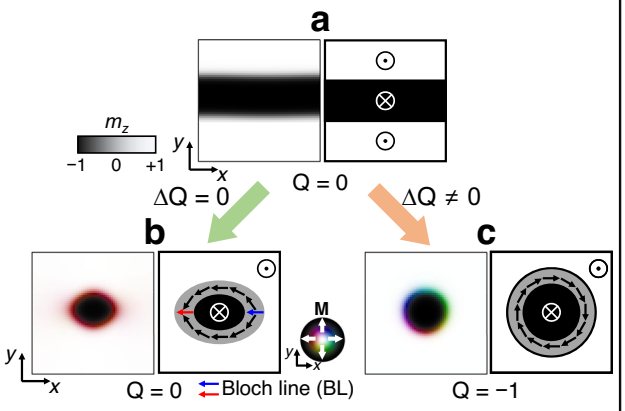

Fig. 1 Representative spin textures in the Fe/Gd multilayer. Magnetization configurations of the topologically trivial stripe domain (**a**), bubble (**b**), and topologically non-trivial skyrmion (**c**). The changes in the topological charge Q of the spin textures are inserted as the stripe domains transition to bubbles and skyrmions.

Results

Spin textures in the Fe/Gd multilayer

Figure 1 shows illustrations of representative spin textures in the Fe/Gd multilayer: stripe domains, bubbles, and skyrmions. The stripe domains are topologically trivial; thus, $Q = 0$ (Fig. 1a). It has been reported that by applying external stimuli such as electrical currents or magnetic fields, stripe domains can be transformed into dot-like spin textures[6,29–32,35–38], such as bubbles (Fig. 1b) or skyrmions (Fig. 1c). The bubble has two Bloch lines (BLs), denoted by red and blue arrows, at the boundary between the bubble core and the outer domain (hereafter, the boundary of the bubble). Topologically, similar to the stripe domains, the Q of a bubble is zero. In contrast, skyrmions have a chiral spin texture characterized by $|Q| = 1$. Notably, broken structural inversion symmetry only occurs between the top and bottom surfaces of multilayers, and its contribution to the emergence of DMI is negligible due to the significant thickness of the overall magnetic medium between the top and bottom surfaces (~90 nm)[32,34,39,40]. In the Fe/Gd multilayers, skyrmions are more likely to be stabilized by dipole–dipole interactions than DMIs[31–34]. As shown in Fig. 1b and c, the shapes of the bubbles and skyrmions created in the Fe/Gd multilayer are distinguishable[6,33–36]. The magnetization configurations of the elliptical- and circular-shaped spin textures obtained by micromagnetic simulations clearly show that the elliptical- and circular-shaped spin textures are bubbles and skyrmions, respectively (Supplementary Information 1). Additionally, we confirmed that the annihilation fields of circular-shaped spin textures are greater than those of elliptical-shaped spin textures by experiments and micromagnetic simulations; our results indicate the higher stability of circular spin textures. The higher (lower) stability of the circular (elliptical)-shaped spin textures supports that the circular (elliptical)-shaped spin textures are topologically non-trivial skyrmions (trivial bubbles). The transition from the stripe domains to bubbles, where Q remains unchanged, is a topologically trivial process. This can be achieved through the continuous transformation of the magnetization configuration in the same homotopy class[1,14]. On the other hand, skyrmions have chiral spin textures characterized by $|Q| = 1$. Therefore, the transition from stripe domains to skyrmions is the topological transition where Q of the entire system changes from $|Q| = 0$ to $|Q| = 1$.

Topological transition triggered by the injection of the magnetic monopole

For an in-depth understanding of the topological transition, we experimentally produced the transition from stripe domains to skyrmions. The initial stripe domains were set by applying a saturation magnetic field of $\mathbf{H} = -0.3$ T, i.e., downward out-of-plane magnetic fields, and then reducing the magnetic field to zero. Considering a previous report that predicts the contribution of the IP magnetic field component to skyrmion generation[6,38,41], we applied magnetic fields slightly tilted by $\theta = 1°$ with respect to the film normal direction, as schematically illustrated in Fig. 2a. In this geometry, due to the tilt angle of magnetic fields with respect to the *z*-axis, a slight magnetic field is also applied to the film plane, i.e., an IP magnetic field. Figure 2b shows the spin textures observed by magnetic transmission soft X-ray microscopy (MTXM) with increasing **H**. All MTXM images were taken at room temperature. The black and white contrasts in the MTXM images represent downward and upward perpendicular magnetizations, respectively. As **H** increases from 0 mT to 162 mT, the stripe domains are transited into circular-shaped skyrmions. As shown in Fig. 1, the circular-shaped

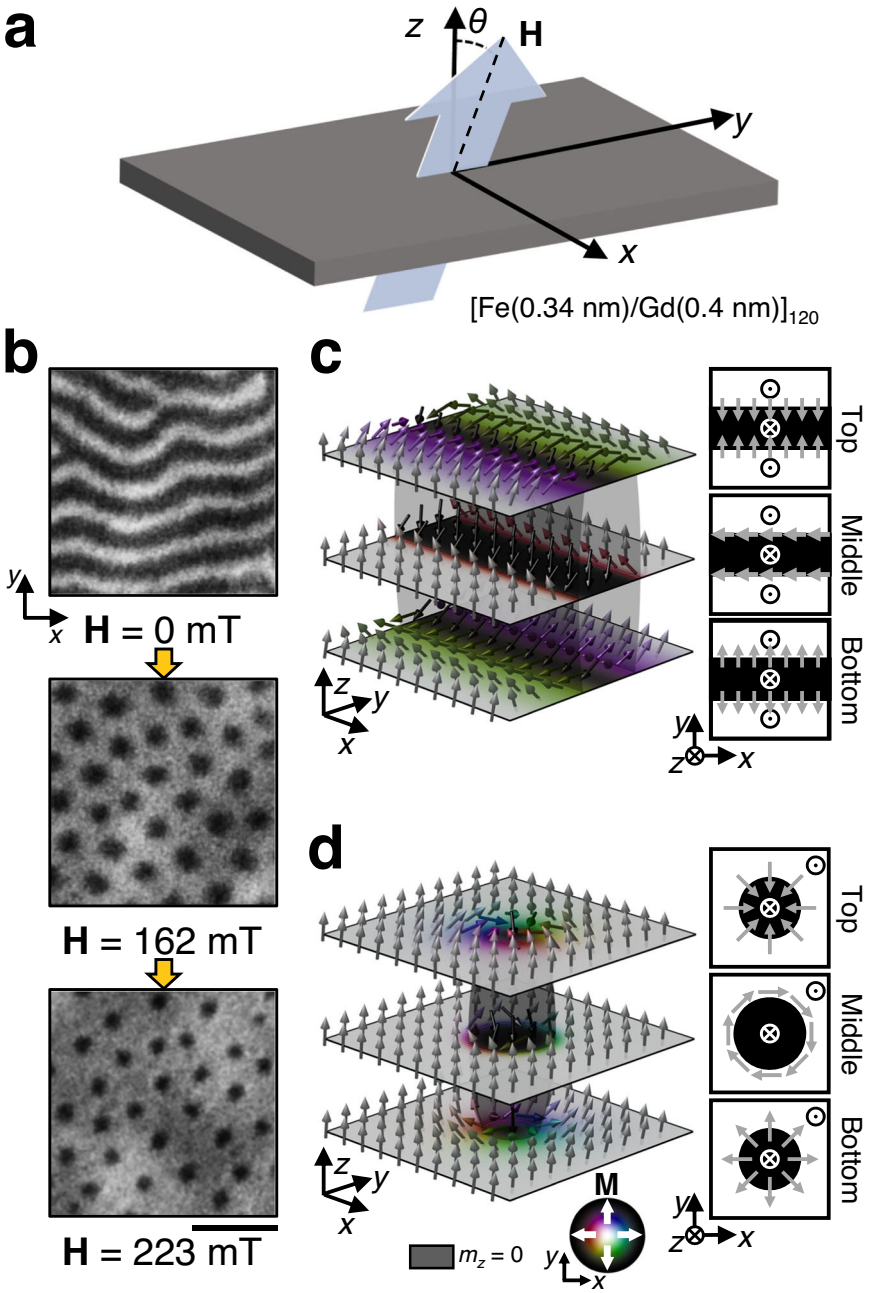

Fig. 2 Topological transition from the stripe domains to skyrmions. a–d, (**a**) Schematic illustration of the model system applying a magnetic field tilted by θ with respect to the *z*-axis. (**b**) Spin textures observed by MTXM with increasing **H** at $\theta = 1°$ (scale bars: 500 nm). Three-dimensional images of the stripe domain (**c**) and skyrmion (**d**) with the schematic images of the magnetization configurations on the top surface, middle region, and bottom surface of the films. The transparent gray surfaces indicate the boundary between upward and downward magnetizations, corresponding to the isosurfaces for $m_z = 0$.

skyrmions can be distinguished from bubbles, which are elliptical-shaped[6,35,36]. As **H** increases further to 223 mT, the skyrmions are reduced in size, but all skyrmions remain and are not annihilated. These results indicate that the high stability of skyrmions is ensured by the non-trivial topology of skyrmions. Figure 2c, d shows the three-dimensional magnetization configurations of the simulated stripe domains and skyrmion, respectively. The transparent gray surfaces indicate the isosurfaces for $m_z = 0$, showing the boundary between upward and downward magnetizations. In the stripe domains (Fig. 2c), flux-closure domain structures are created with respect to the domain walls to

reduce the demagnetization energy (Supplementary Information 2); here, the domain walls on the top and bottom surfaces of the film become right- and left-handed Néel walls, respectively. Interestingly, however, in the middle region of the film, Bloch walls where the magnetizations are oriented toward the x-axis are generated to avoid high exchange energy in the region. In the stripe domain created by applying magnetic fields with a tilt angle of 1° with respect to the z-axis, magnetizations of domain walls in the middle region of the film are found to be aligned in the $-x$-direction, as shown in Fig. 2c. For the skyrmion (Fig. 2d), the flux-closure domain structures lead to Néel configurations on top and bottom surfaces with opposite chirality, while the middle region of the film shows the Bloch configuration (Supplementary Information 2).

The mechanism of the experimentally observed topological transition from stripe domains to skyrmions was investigated in detail using micromagnetic simulations (Fig. 3a and Supplementary Movie 1). The initial stripe domain starts breaking as **H** increases. However, we found that the stripe domain is not directly transformed into a skyrmion. Surprisingly, a bubble with two BLs, indicated by blue and red arrows, transiently appears immediately after the stripe domain breaks (snapshot at $t = 2.45$ ns). The magnetizations at the blue and red BLs are aligned in the same $-x$ direction as those of domain walls in the stripe domain. Notably, the magnetization configurations around the two BLs on the top and bottom surfaces are different. On the top surface, the spatial variation in the magnetization around the red BL is more drastic than the spatial variation in the magnetization around the blue BL. On the other hand, on the bottom surface, the magnetizations around the blue BL are spatially more inhomogeneous than the magnetizations around the red BL. We found that the difference between magnetizations around the red and blue BLs on the top and bottom surfaces is closely associated with dipole–dipole interactions (Supplementary Information 1). Once a bubble is formed, however, two MPs, denoted by the blue and red spheres, are injected into the BLs with drastically varying magnetization (i.e., the red BL on the top surface and the blue BL on the bottom surface). By the injection of the MPs, which involves the annihilation of the red BL on the top surface and the blue BL on the bottom surface, the magnetization configurations on the top and bottom surfaces are changed to that of the skyrmion, as depicted in the 2D schematic images of the snapshot at $t = 2.60$ ns. The MPs injected from the top and bottom surfaces exhibit convergent and divergent magnetization configurations, which are topologically characterized by $Q_{\frac{MP}{Top}} = -1$ and $Q_{\frac{MP}{Top}} = +1$, respectively. The injected MPs propagate through the boundary of the bubble, as indicated by the cyan and magenta lines (snapshot at $t = 5.10$ ns). When the MPs reach the middle region of the film, they start moving toward each other in the middle region of the film (snapshot at $t = 5.68$ ns). The movement of the MPs is accompanied by magnetization switching, which converts magnetizations at the boundary of the bubble to those of the skyrmion in the middle region of the film. The micromagnetic simulation results for the detailed magnetization switching process in the middle region of the film are illustrated in Supplementary Information 3. Interestingly, despite the non-trivial topology of MPs, when the MPs collide with each other, they are annihilated together, completing the topological transition from the stripe domain to the skyrmion (snapshot at $t = 6$ ns). Since two MPs have opposite topological charges ($Q^{MP}_{Bot} + Q^{MP}_{Top} = 0$), pair annihilation of MPs is a topologically trivial process, as shown in Fig. 3b. The results in Fig. 3 clearly show that the topological transition from the stripe domain to the skyrmion is achieved through the sequential processes of the injection, propagation, and paired annihilation of MPs.

On the basis of extensive micromagnetic simulations with various magnetic field configurations, we found that the topological transition from stripe domains to skyrmions is most reliable when a magnetic field slightly tilted along the $+x$-axis is applied rather than when only a magnetic field is applied along the $+z$-axis (Supplementary Information 4), as was done in the experiments shown in Fig. 2. These results indicate that the IP magnetic field induced by applying magnetic fields at an angle tilted by 1° toward the $+x$-axis (Fig. 2a) might be key to manipulating the MP injection. Indeed, the IP magnetic field has been discussed as playing an important role in generating skyrmions and having a decisive influence on the shape of the spin textures[6,41–43].

Role of in-plane magnetic fields in the injection of magnetic monopoles

To clearly verify the role of the IP magnetic field in MP injection, we examined the transition from the bubble to the skyrmion by directly applying a magnetic field, H_x, along the film plane (x-direction). To stably form bubbles in magnetic media, we applied an out-of-plane magnetic field of $H_z = 280$ mT. Under fixed H_z, the IP magnetic field increased from $H_x = -20$ mT. Figure 4a shows the magnetization configurations of the bubbles (snapshots at $H_x = -20$ mT, 0 mT, and 1.4 mT) and skyrmions (snapshot at $H_x = 1.5$ mT), along with the exchange energy density of these configurations (Fig. 4b). Here, the magnetization at the BL in the bubble is also aligned in the $-x$-direction. When the IP magnetic field increases from $H_x = -20$ mT to $H_x = 0$ mT, the magnetizations at the BLs become more inhomogeneous (snapshot at $H_x = 0$ mT). As a result, the corresponding exchange energy becomes much greater at the red BL on the top surface and the blue BL on the bottom surface. When the IP

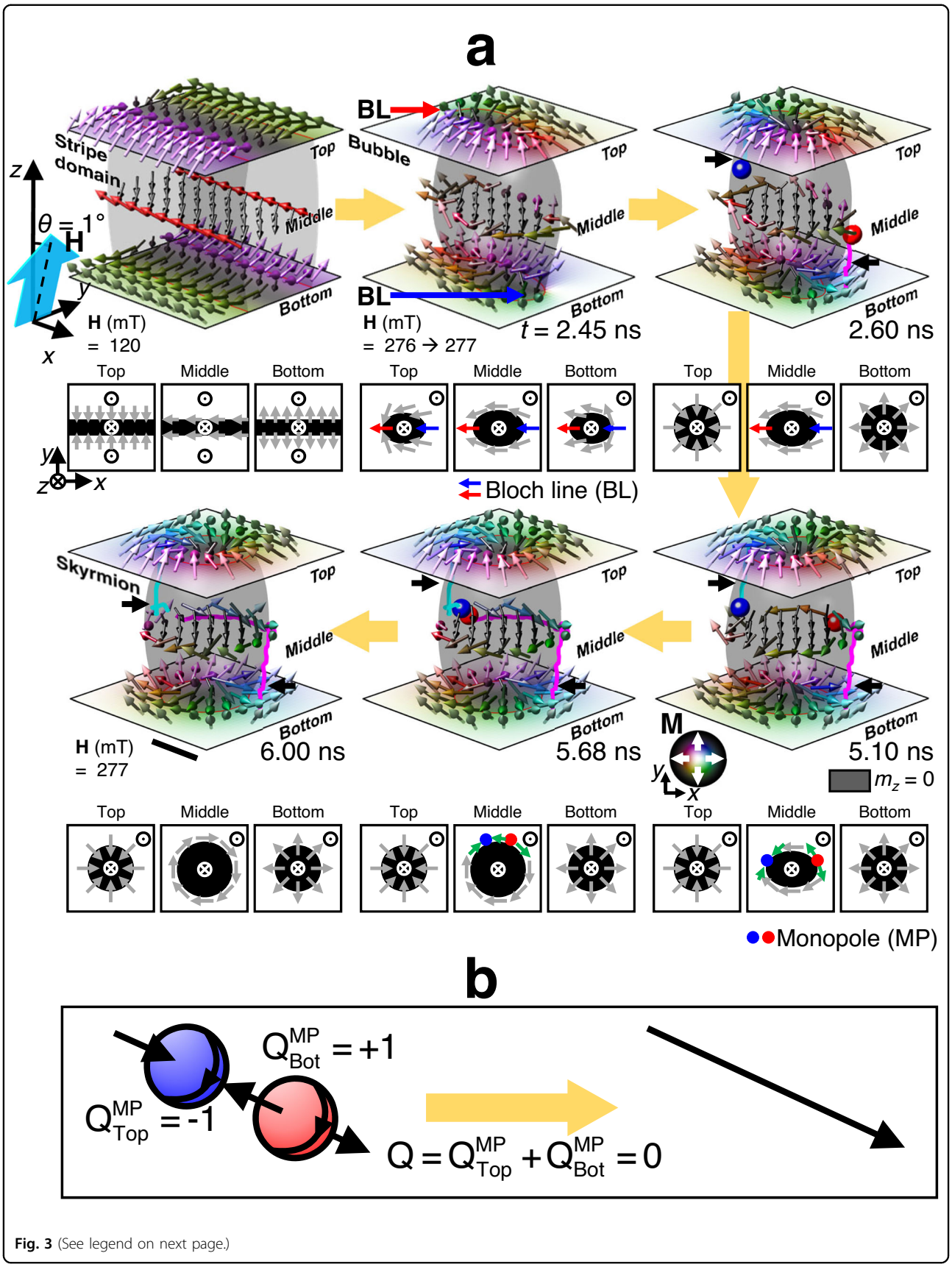

Fig. 3 (See legend on next page.)

(see figure on previous page)

Fig. 3 MP injection in the topological transition. a, **b**, (**a**) Process of the topological transition from the stripe domain to the skyrmion at $\theta = 1°$ (scale bar: 30 nm). The schematic images of the magnetization configurations on the top surface, middle region, and bottom surface of the films are inserted below the three-dimensional illustration of the magnetization configurations. The red and blue arrows indicate the BLs in the bubble. The red and blue spheres indicate the MPs injected from the bottom and top surfaces; these are topologically characterized by $Q_{Top}^{MP} = -1$ and $Q_{Bot}^{MP} = +1$, respectively. The trajectories of red and blue MPs are denoted by magenta and cyan lines, respectively. **b** Schematic illustrations of the pair annihilation of the injected MPs.

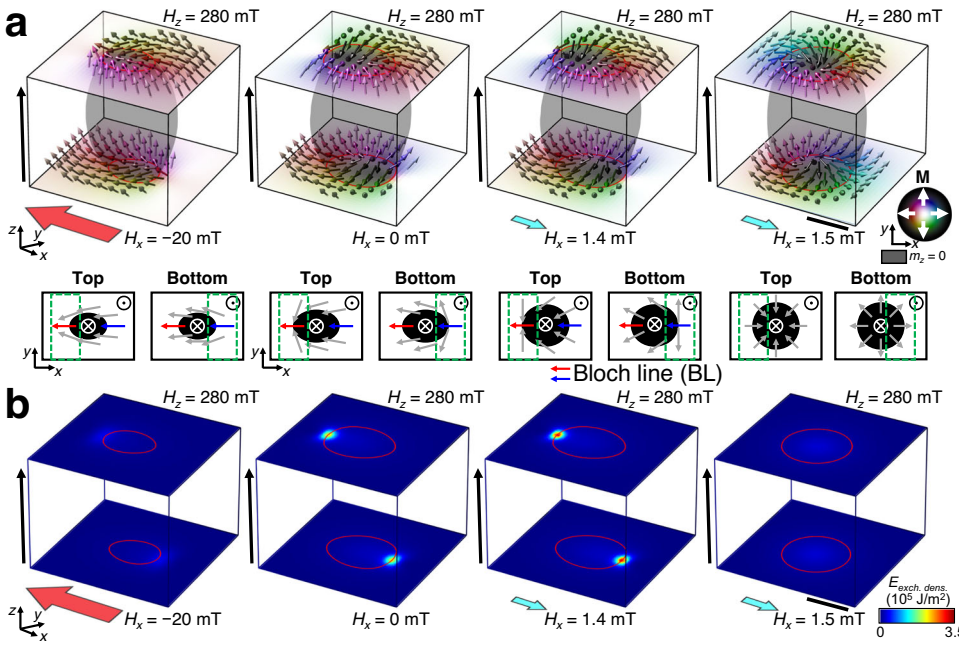

Fig. 4 Role of IP magnetic fields in MP injection. Magnetization configuration of the spin texture (**a**) and exchange energy density ($E_{exch.\ dens.}$) (**b**) under perpendicular magnetic fields of $H_z = 280$ mT as the IP magnetic field of H_x is swept from −20 mT to 1.5 mT (scale bars: 30 nm). The schematic images describing the magnetization configuration on the top and bottom surfaces were inserted below the three-dimensional illustration of the spin textures. The red and blue arrows indicate the BLs. The green dashed boxes indicate that the BLs have relatively large inhomogeneous magnetizations.

magnetic field is applied in the $+x$-direction, opposite to the magnetization at the BLs, and increases to 1.4 mT, the exchange energy at those BLs significantly increases (snapshot at $H_x = 1.4$ mT) because of the drastic spatial inhomogeneity of the magnetizations at those BLs. A further increase in H_x to 1.5 mT finally leads to the transition from the bubble to the skyrmion with the relaxation of the exchange energy. In the transition process, MPs are injected from surfaces, and the BLs are annihilated. The exchange energy at the BLs is converted into energy for the injection of MP to reduce the total energy of the system[22]. The results in Fig. 4 clearly confirm that the IP magnetic field triggers MP injection by concentrating the local exchange energy at the BLs. Additionally, Fig. 4 shows that a certain strength of the IP magnetic field, $H_x = 1.5$ mT, is required for MP injection, indicating that MP injection can be manipulated by adjusting the strength of the IP magnetic field.

Controlled injection of the magnetic monopole in the topological transition

To experimentally confirm whether the MP injection is controllable by varying the strength of the IP magnetic field, we applied magnetic fields tilted toward the $+x$-axis with various θ to manipulate the strength of the IP magnetic field and observed the spin textures (Fig. 2a). θ is varied from 1° to 10° in steps of 1° (Supplementary Information 5). Figure 5a shows spin textures observed at $\mathbf{H} = 0$ mT, 162 mT, and 206 mT with $\theta = 1°$, 3°, 5°, 7°, and 9°, respectively. H_x corresponds to the strength of the IP magnetic field induced by $\mathbf{H}$ with θ. We observed that the stripe domains break into dot-like spin textures at $\mathbf{H} = 162$ mT. Some of the dot-like spin textures at $\mathbf{H} = 162$ mT are circular-shaped skyrmions, while others are elliptical-shaped bubbles (for example, $\theta = 7°$ and 9°). As $\mathbf{H}$ increases to 206 mT, the topologically protected circular-shaped skyrmions remain stable, while the elliptical-shaped bubbles are annihilated, which supports the

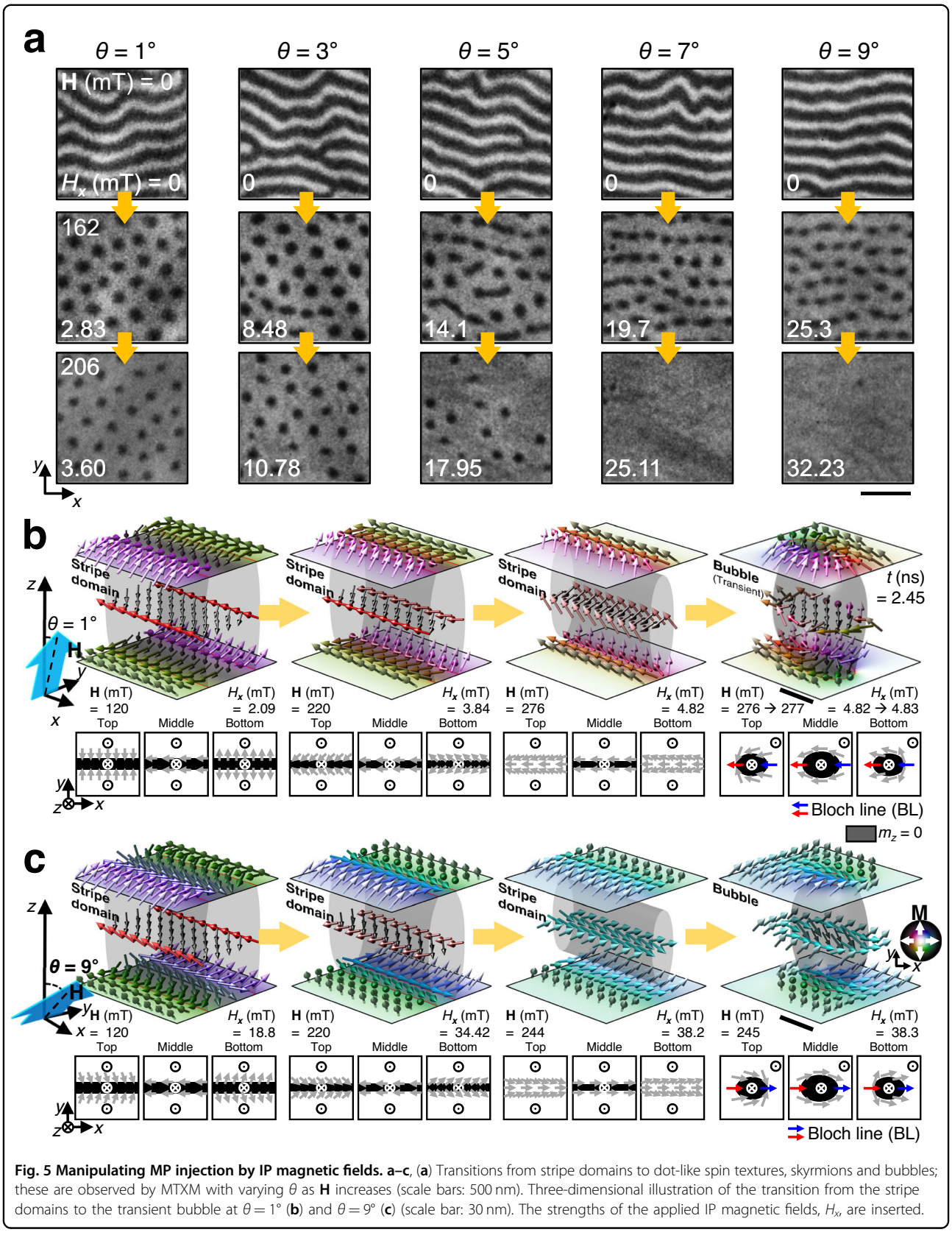

Fig. 5 Manipulating MP injection by IP magnetic fields. a–c, (**a**) Transitions from stripe domains to dot-like spin textures, skyrmions and bubbles; these are observed by MTXM with varying θ as **H** increases (scale bars: 500 nm). Three-dimensional illustration of the transition from the stripe domains to the transient bubble at $\theta = 1°$ (**b**) and $\theta = 9°$ (**c**) (scale bar: 30 nm). The strengths of the applied IP magnetic fields, H_x, are inserted.

greater stability of skyrmions than bubbles. The experimentally observed differences in the annihilation fields of the skyrmions and bubbles were also confirmed by micromagnetic simulations (Supplementary Information 6). Remarkably, the populations of skyrmions and bubbles strongly depend on θ and can be determined by counting the number of dot-like spin textures remaining at $\mathbf{H} = 206$ mT. At $\theta = 1°$, only skyrmions are formed, whereas only bubbles are formed at $\theta \geq 7°$ since no remaining spin texture is present. Note that the circular structures observed at $\theta = 7°$ and 9° and at high **H** were confirmed to be defects (Supplementary Information 7). At $1° < \theta < 7°$, skyrmions and bubbles coexist, and as θ increases, the population of skyrmions decreases while the population of bubbles increases. The results in Fig. 5a show that the topological transition from stripe domains into skyrmions occurs only at weak IP magnetic fields ($\theta = 1°$ and $H_x = 2.83$ mT); these results indicate that MP injection is triggered when the applied IP magnetic field is relatively weak ($\theta = 1°$ and $H_x = 2.83$ mT) but is hindered when a strong IP magnetic field ($\theta > 7°$ and $H_x > 19.7$ mT) is applied.

To understand the MP injection process that occurs as a function of the strength of the IP magnetic field, we thoroughly investigated the process by which the stripe domain is converted into a bubble. Figure 5b, c shows the magnetization process in which the stripe domain converts to the transient bubble at $\theta = 1°$ and $\theta = 9°$, respectively. By applying the magnetic field at $\theta = 1°$, the magnetizations of the domain walls in the stripe domain on the top and bottom surfaces are tilted in the $-x$-direction along with those in the middle region of the film. The magnetization direction of the domain walls and that at the BLs in the transient bubble remain the same in the $-x$-direction. On the other hand, with the applied magnetic field at $\theta = 9°$, due to the relatively strong IP magnetic field induced, the magnetization direction of the domain walls in the stripe domain on the top and bottom surfaces and in the middle region of the film are flipped from the $-x$-direction into the $+x$-direction. As a result, in the transient bubble formed at $\theta = 9°$, the magnetization directions in the boundary and BLs in the transient bubble are aligned in the $+x$-direction. Since the magnetization at the BLs in the transient bubble formed at $\theta = 1°$ is aligned in the $-x$-direction, which is opposite to the direction of the IP magnetic field ($+x$-direction), the exchange energy at the BLs in the bubble is highly localized and increases with increasing IP magnetic field; thus, MP injection is triggered at the BLs, as shown in Fig. 4. However, the magnetization at the BLs in the transient bubble formed at $\theta = 9°$ is parallel to the direction of the IP magnetic field ($+x$-direction). Therefore, the applied IP magnetic field reduces the exchange energy at the BLs, unlike in the case of $\theta = 1°$; thus, the bubble is stabilized and is the final spin texture without MP injection. The experimental results in Fig. 5 strongly support that MP injection can be effectively and simply controlled by adjusting the tilt angle of the applied magnetic field, i.e., the strength of the IP magnetic field.

Conclusion

In summary, we report a well-manipulated injection of MPs leading to the topological transition from the stripe domain to the skyrmion by applying a slightly tilted magnetic field to the film surface of an Fe/Gd multilayer. The mechanism of MP injection during topological transition was thoroughly examined, and it was found that the MP injection strongly depended on the strength of the IP magnetic field. We experimentally demonstrated that MP injection could be effectively controlled by applying IP magnetic fields to Fe/Gd multilayer. Our findings on controllable MP injection can be extended to manipulate and examine the topological transitions between various topological spin textures.

Materials and methods

Sample fabrication

The $[Fe(0.34\,nm)/Gd(0.4\,nm)]_{120}$ ferrimagnetic multilayer film was fabricated by magnetron sputtering. Then, 0.34-nm-thick Fe and 0.4-nm-thick Gd layers were alternately deposited on a 100-nm-thick X-ray transparent Si_3N_4 membrane substrate.

X-ray imaging technique

The magnetic components in the $[Fe(0.34\,nm)/Gd(0.4\,nm)]_{120}$ ferrimagnetic multilayer film were directly observed by utilizing full-field magnetic transmission X-ray microscopy (MTXM) at the Beamline 6.1.2 in the Advanced Light Source (ALS)[44]. Out-of-plane magnetic components were imaged at the Fe L_3 X-ray absorption edge (708 eV). All MTXM measurements were performed at room temperature. To apply the IP magnetic field, the sample holder was tilted with respect to the out-of-plane magnetic field.

Micromagnetic simulation

To specify the detailed magnetization configurations in the Fe/Gd multilayer film, we performed a micromagnetic simulation utilizing the MuMax[3] code, and typical material parameters of Fe/Gd multilayer films were used, with the following parameters: a saturation magnetization $M_s = 400$ kA/m, an exchange stiffness $A_{ex} = 5$ pJ/m, and a uniaxial anisotropy $K_u = 40\,kJ/m^3$. We numerically solved the Landau–Lifshitz–Gilbert (LLG) equation $\partial\mathbf{M}/\partial t = -\gamma_0(\mathbf{M}\times\mathbf{H}_{eff}) + (\alpha/|\mathbf{M}|)(\mathbf{M}\partial\mathbf{M}/\partial t)$ with the local magnetization vector **M**, the gyromagnetic ratio γ_0, the effective field $\mathbf{H}_{eff}$, and the phenomenological damping constant α using the MuMax[3] code[45–47]. To study the MP injection process, we carried out quasistatic calculations where the precessional effects were excluded and the

damping constant α was set to 0.5. We used 300 × 300 × 100 nm^3 films with periodic boundary conditions.

Acknowledgements
Research at the ALS was supported by the U.S. Department of Energy (DE-AC02-05CH11231). M.-Y.I. acknowledges support from Lawrence Berkeley National Laboratory through the Laboratory Directed Research and Development (LDRD) Program. S.-G.J. was supported by the National Research Foundation of Korea grant funded by the Korea government (NRF-2020R1C1C1006194). K.-S.L. was supported by the NRF grant funded by the Korea government (MSIT) (RS-2023-00217968 and 2020M3F3A2A03082987), the 2023 Research Fund (1.230013.01 and 1.230063.01) of UNIST (Ulsan National Institute of Science and Technology), and the Korea Institute for Advancement of Technology (KIAT) grant funded by the Korea Government (MOTIE) (P0023703, HRD Program for Industrial Innovation). Research at UC San Diego was supported by the U.S. National Science Foundation (NSF) under the award from the National Science Foundation, Division of Materials Research Award 2105401. S.A.M. acknowledges support from the U.S. Department of Defense.

Author details
[1]Center for X-ray Optics, Lawrence Berkeley National Laboratory, Berkeley, CA 94720, USA. [2]Department of Materials Science and Engineering, Korea National University of Transportation, Chungju 27469, Republic of Korea. [3]Center for Memory and Recording Research, University of California San Diego, La Jolla, CA 92093, USA. [4]Department of Physics, Chonnam National University, Gwangju 61186, Republic of Korea. [5]Department of Materials Science and Engineering, Ulsan National Institute of Science and Technology (UNIST), Ulsan 44919, Republic of Korea. [6]Graduate School of Semiconductor Materials and Devices Engineering, Ulsan National Institute of Science and Technology (UNIST), Ulsan 44919, Republic of Korea

Author contributions
H.-S.H., S.-G.J., K.-S.L., and M.-Y.I. designed and planned the research. H.-S.H., S.-G.J., W.C., and M.-Y.I. carried out the magnetic transmission soft X-ray microscopy experiments. S.A.M. and E.E.F. prepared the samples. H.-S.H. and S.-G.J. analyzed the data. H.-S.H. carried out the micromagnetic simulations. H.-S.H., S.-G.J., M.-Y.I., and K.-S.L. prepared the manuscript; additionally, the manuscript incorporates critical input from all authors.

Data availability
The data that support the findings of this study are available from the corresponding author upon reasonable request.

Conflict of interest
The authors declare no competing interests.

Publisher's note
Springer Nature remains neutral with regard to jurisdictional claims in published maps and institutional affiliations.

Supplementary information The online version contains supplementary material available at https://doi.org/10.1038/s41427-024-00529-9.

Received: 25 April 2023 Revised: 12 December 2023
Accepted: 19 December 2023
Published online: 16 February 2024

References

1. Braun, H.-B. Topological effects in nanomagnetism: from superparamagnetism to chiral quantum solitons. *Adv. Phys.* **61**, 1–116 (2012).
2. Nagaosa, N. & Tokura, Y. Topological properties and dynamics of magnetic skyrmions. *Nat. Nanotechnol.* **8**, 899–911 (2013).
3. Hagemeister, J., Romming, N., von Bergmann, K., Vedmedenko, E. Y. & Wiesendanger, R. Stability of single skyrmionic bits. *Nat. Commun.* **6**, 8455 (2015).
4. Muckel, F. et al. Experimental identification of two distinct skyrmion collapse mechanisms. *Nat. Phys.* **17**, 395–402 (2021).
5. Oike, H. et al. Interplay between topological and thermodynamic stability in a metastable magnetic skyrmion lattice. *Nat. Phys.* **12**, 62–66 (2016).
6. Je, S.-G. et al. Direct demonstration of topological stability of magnetic skyrmions via topology manipulation. *ACS Nano* **14**, 3251–3258 (2020).
7. Jiang, W. et al. Direct observation of the skyrmion Hall effect. *Nat. Phys.* **13**, 162–169 (2017).
8. Litzius, K. et al. Skyrmion Hall effect revealed by direct time-resolved X-ray microscopy. *Nat. Phys.* **13**, 170–175 (2017).
9. Yang, S. et al. Magnetic skyrmion transistor gated with voltage-controlled magnetic anisotropy. *Adv. Mater.* **35**, 2208881 (2022).
10. Yu, X. Z. et al. Transformation between meron and skyrmion topological spin textures in a chiral magnet. *Nature* **564**, 95–98 (2018).
11. Fujishiro, Y. et al. Topological transitions among skyrmion- and hedgehog-lattice states in cubic chiral magnets. *Nat. Commun.* **10**, 1059 (2019).
12. Zhou, Y. & Ezawa, M. A reversible conversion between a skyrmion and a domain-wall pair in a junction geometry. *Nat. Commun.* **5**, 4652 (2014).
13. Tretiakov, O. A. & Tchernyshyov, O. Vortices in thin ferromagnetic films and the skyrmion number. *Phys. Rev. B* **75**, 012408 (2007).
14. Mermin, N. D. The topological theory of defects in ordered media. *Rev. Mod. Phys.* **51**, 591–648 (1979).
15. Feldtkeller, E. Mikromagnetisch stetige und unstetige Magnetisierungskonfigurationen. *Z. Angew. Phys* **19**, 530–536 (1965).
16. Döring, W. Point singularities in micromagnetism. *J. Appl. Phys.* **39**, 1006–1007 (1968).
17. Kim, S. K. & Tchernyshyov, O. Pinning of a Bloch point by an atomic lattice. *Phys. Rev. B* **88**, 174402 (2013).
18. Han, H.-S. et al. Topology-dependent stability of vortex-antivortex structures. *Appl. Phys. Lett.* **118**, 212407 (2021).
19. Im, M.-Y. et al. Dynamics of the Bloch point in an asymmetric permalloy disk. *Nat. Commun.* **10**, 593 (2019).
20. Hierro-Rodriguez, A. et al. Revealing 3D magnetization of thin films with soft X-ray tomography: magnetic singularities and topological charges. *Nat. Commun.* **11**, 6382 (2020).
21. Donnelly, C. et al. Three-dimensional magnetization structures revealed with X-ray vector nanotomography. *Nature* **547**, 328–331 (2017).
22. Thiaville, A., García, J. M., Dittrich, R., Miltat, J. & Schrefl, T. Micromagnetic study of Bloch-point-mediated vortex core reversal. *Phys. Rev. B* **67**, 094410 (2003).
23. Wartelle, A. et al. Bloch-point-mediated topological transformations of magnetic domain walls in cylindrical nanowires. *Phys. Rev. B* **99**, 024433 (2019).
24. Beg, M. et al. Stable and manipulable Bloch point. *Sci. Rep.* **9**, 7959 (2019).
25. Van Waeyenberge, B. et al. Magnetic vortex core reversal by excitation with short bursts of an alternating field. *Nature* **444**, 461–464 (2006).
26. Noske, M., Stoll, H., Fähnle, M., Hertel, R. & Schütz, G. Mechanisms for the symmetric and antisymmetric switching of a magnetic vortex core: Differences and common aspects. *Phys. Rev. B* **91**, 014414 (2015).
27. Hertel, R., Gliga, S., Fähnle, M. & Schneider, C. M. Ultrafast nanomagnetic toggle switching of vortex cores. *Phys. Rev. Lett.* **98**, 117201 (2007).
28. Hertel, R. & Schneider, C. M. Exchange explosions: Magnetization dynamics during vortex-antivortex annihilation. *Phys. Rev. Lett.* **97**, 177202 (2006).
29. Jiang, W. et al. Blowing magnetic skyrmion bubbles. *Science* **349**, 283–286 (2015).
30. Milde, P. et al. Unwinding of a skyrmion lattice by magnetic monopoles. *Science* **340**, 1076–1080 (2013).
31. Montoya, S. A. et al. Tailoring magnetic energies to form dipole skyrmions and skyrmion lattices. *Phys. Rev. B* **95**, 024415 (2017).
32. Montoya, S. A. et al. Resonant properties of dipole skyrmions in amorphous Fe/Gd multilayers. *Phys. Rev. B* **95**, 224405 (2017).
33. Chess, J. et al. Observation of skyrmions at room-temperature in amorphous Fe/Gd films. *Microscopy Microanal.* **21**, 1649–1650 (2015).
34. Parker, W., Montoya, S., Fullerton, E. & McMorran, B. Chiral spin textures in Fe/Gd based multilayer thin films. *Microscopy Microanal.* **27**, 2404–2407 (2021).
35. Turnbull, L. A. et al. Tilted X-Ray holography of magnetic bubbles in MnNiGa Lamellae. *ACS Nano* **15**, 387–395 (2021).
36. Loudon, J. C. et al. Do images of Biskyrmions show Type-II bubbles? *Adv. Mater.* **31**, 1806598 (2019).
37. Woo, S. et al. Spin-orbit torque-driven skyrmion dynamics revealed by time-resolved X-ray microscopy. *Nat. Commun.* **8**, 15573 (2017).

38. Moon, K.-W. et al. Universal method for magnetic skyrmion bubble generation by controlling the stripe domain instability. *NPG Asia Mater.* **13**, 20 (2021).
39. Legrand, W. et al. Hybrid chiral domain walls and skyrmions in magnetic multilayers. *Sci. Adv.* **4**, eaat0415 (2018).
40. Cui, B. et al. Néel-Type Elliptical skyrmions in a laterally asymmetric magnetic multilayer. *Adv. Mater.* **33**, 2006924 (2021).
41. Yang, S. et al. Magnetic field magnitudes needed for skyrmion generation in a general perpendicularly magnetized film. *Nano Lett.* **22**, 8430–8436 (2022).
42. Han, H.-S. et al. Tuning of oscillation modes by controlling dimensionality of spin structures. *NPG Asia Mater.* **14**, 91 (2022).
43. Ding, B. et al. Manipulating spin chirality of magnetic skyrmion bubbles by in-plane reversed magnetic fields in $(Mn_{1-x}Nix)_{65}Ga_{35}$ ($x = 0.45$) magnet. *Phys. Rev. Appl.* **12**, 054060 (2019).
44. Fischer, P. et al. Soft X-ray microscopy of nanomagnetism. *Mater. Today* **9**, 26–33 (2006).
45. Gilbert, T. L. A Lagrangian formulation of the gyromagnetic equation of the magnetization field. *Phys. Rev.* **100**, 1243 (1955).
46. Landau, L. D. & Lifshitz, E. M. On the theory of the dispersion of magnetic permeability in ferromagnetic bodies. *Phys. Z. Sowjetunion* **8**, 153–164 (1955).
47. Vansteenkiste, A. et al. The design and verification of MuMax3. *AIP Adv.* **4**, 107133 (2014).